Large Counterions Boost the Solubility and Renormalized Charge of Suspended Nanoparticles

Guillermo Iván Guerrero-García,[†] Pedro González-Mozuelos,[‡] and Monica Olvera de la Cruz[†,§,*]

[†]Department of Materials Science and Engineering, Northwestern University, Evanston, Illinois 60208, United States, [‡]Departamento de Física, Cinvestav del I.P.N., Avenida Instituto Politécnico Nacional 2508, Distrito Federal, C.P. 07360, Mexico, and [§]Department of Chemical Engineering, Northwestern University, Evanston, Illinois 60208, United States

ABSTRACT Colloidal particles are ubiquitous in biology and in everyday products such as milk, cosmetics, lubricants, paints, or drugs. The stability and aggregation of colloidal suspensions are of paramount importance in nature and in diverse nanotechnological applications, including the fabrication of photonic materials and scaffolds for biological assemblies, gene therapy, diagnostics, targeted drug delivery, and molecular labeling. Electrolyte solutions have been extensively used to stabilize and direct the assembly of colloidal particles. In electrolytes, the effective electrostatic interactions among the suspended colloids can be changed over various length scales by tuning the ionic concentration. However, a major limitation is gelation or flocculation at high salt concentrations. This is explained by classical theories, which show that the electrostatic repulsion among charged colloids is significantly reduced at high electrolyte concentrations. As a result, these screened colloidal particles are expected to aggregate due to short-range attractive interactions or dispersion forces as the salt concentration increases. We discuss here a robust, tunable mechanism for colloidal stability by which large counterions prevent highly charged nanoparticles from aggregating in salt solutions with concentrations up to 1 M. Large counterions are shown to generate a thicker ionic cloud in the proximity of each charged colloid, which strengthens short-range repulsions among colloidal particles and also increases the corresponding renormalized colloidal charge perceived at larger separation distances. These effects thus provide a reliable stabilization mechanism in a broad range of biological and synthetic colloidal suspensions.

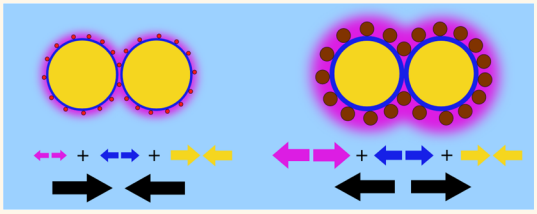

KEYWORDS: colloidal stability · charged nanoparticles · renormalized charges

Colloidal suspensions are ubiquitous in biological systems, with blood being just one example. They are also common in daily products such as milk, cosmetics, lubricants, paints, and drugs. Moreover, colloidal suspensions of charged nanoparticles have important technological and environmental science applications. Recently, they have been shown to be ideal for the fabrication of photonic materials and scaffolds for biological assemblies, gene therapy, diagnostics, targeted drug delivery, and molecular labeling.[1−5] One important limitation often found in the use of colloidal solutions is their propensity to aggregate or flocculate. For this reason, a large number of studies devoted to control the stability of colloids in solution has emerged. In many of these investigations, the solvent is often assumed to be a continuum that mediates the effective interactions among the solute particles. It is thus very important to be able to compute the effective pair potential between the suspended nanoparticles in order to control their assembly properties. Furthermore, since in numerous biological and industrial processes diverse degrees of solubility are required at different stages, a simple and effective tunable mechanism for promoting or inhibiting aggregation in colloidal suspensions, based on our current theoretical understanding, is highly desirable.

In charged colloidal suspensions, the ionic strength of the electrolyte has been widely used to disperse or drive the crystallization of the suspended particles *via* electrostatics. This mechanism is very appealing because a large number of directed assemblies depend on the competition of short-range attractions and long-range repulsions among similar charged colloids. In addition, long-range electrostatic interactions can be tuned externally by controlling the ionic

* Address correspondence to m-olvera@northwestern.edu.

Received for review June 3, 2013 and accepted November 1, 2013.

Published online November 01, 2013
10.1021/nn404477b

strength and composition of the electrolyte, thus allowing to achieve specific structures in a wide variety of biological and synthetic colloidal solutions.

Traditionally, the Derjaguin–Landau–Verwey–Overbeek (DLVO) theory[6,7] has been the standard theoretical framework used to describe the stability and coagulation regimes of colloidal solutions in electrolytes. Nevertheless, the DLVO theory is based on the linearized Poisson–Boltzmann (PB) equation of point-like ions,[8] which neglects ion correlations, excluded volume of ions, polarization, and hydrophobic effects. Ion correlations and excluded volume effects[9,10] play a fundamental role in interesting phenomena such as like-charge attraction[11,12] and inversion of the electrophoretic mobility.[13] Polarization effects[14] are very relevant in the presence of dielectric discontinuities and multivalent ions,[15,16] and the coagulation properties of hydrophobic colloids may depend significantly on the hydrophobicity or hydrophilicity of the supporting electrolyte.[17] Despite the limitations of the PB approach, the DLVO theory is usually the first choice to fit experimental results by simply replacing the original bare charge with an effective charge of lower magnitude.[18−20] Several theories have been proposed to calculate *a priori* the corresponding effective charges.[21−23] However, these approaches need to be modified when ion correlations and excluded volume effects become relevant.

Excluded volume effects and ion correlations have been extensively analyzed in the context of the precipitation and redissolution of polyelectrolytes as the concentration of multivalent salt increases.[24−26] This reentrant transition, which is also observed in DNA[11,27] and in proteins,[28] is a function not only of the charge of the macroions but also of the relative size of counterions and co-ions, as shown by theory[26,29] and corroborated by simulations.[30] Relative size effects of counterions to co-ions can also occur in colloidal suspensions in the presence of monovalent salts.[31−33] In particular, computer simulations and theoretical calculations suggest that ion correlations and excluded volume effects can induce a counterion-driven short-range attraction between highly charged nanoparticles in concentrated size-asymmetric monovalent electrolytes.[34] Experimentally, this behavior as well as charge inversion[35] can easily be masked by short-range van der Waals attractive interactions that are usually present at the nanoscale.[36] In the presence of large counterions and small co-ions at high electrolyte concentrations, however, an enhanced short-range repulsion between highly charged nanoparticles can be inferred from simulations and theory in comparison to the DLVO results.[34] This possibility has profound consequences in the physical properties of colloidal dispersions, including an enhanced stabilization of highly charged nanoparticles in concentrated salts, which has been observed experimentally.[37]

The goal of this paper is to investigate how and to what extent ion correlations and excluded volume effects due to large counterions modify the stability of highly charged colloids. To this end, we study the role of the counterion size on the effective interactions between charged nanoparticles in the same situations where the classical DLVO theory predicts that short-range van der Waals attractions overcome the highly screened electrostatic repulsion between like-charged colloids, thus inducing their coagulation. Larger counterions are shown to enhance the stability of the suspension by considerably increasing the effective short-range repulsions between macroions. The mechanism behind this seems to be a less efficient electrostatic shielding coming from the combination of large counterions and small co-ions. This is confirmed by the analysis of the renormalized macroion charges and screening lengths that regulate the long-range behavior of the macroion–macroion interaction. In particular, these renormalized charges are coupled to the short-range shielding of the bare macroion charge *via* a set of exact general relations,[38−40] thereby propagating the details of the ionic distribution in the vicinity of each macroion to large separation distances.

The present study is focused on interactions among suspended charged nanoparticles. The mechanisms described here, however, are more general and should be applicable not only to this length scale but also to larger highly charged colloids.[41−47] Moreover, these mechanisms may be fine-tuned by the right mixture of counterion sizes in a multicomponent electrolyte solution, thus allowing tighter control of the colloidal stability for a wide variety of liquid suspensions during ongoing industrial and biotechnological processes.

MODEL SYSTEM

The influence of large counterions on the effective interactions between highly charged colloids is studied here by considering two spherical anionic hydrophilic nanoparticles, of diameter d_M and constant surface charge density, immersed in various 1:1 aqueous electrolytes with different counterion to co-ion ratios. In order to access computationally several salt concentrations and to minimize the number of system-specific parameters, we use a coarse-grained approach based on the primitive model. In this scheme, solvent molecules are replaced by a continuous medium, and the nanoparticles and the ions are modeled as repulsive-core spheres with point charges at their centers. To study the effect of different size-asymmetric monovalent electrolytes at high salt concentrations, we consider small Na cations and large tetraalkylammonium cations with different hydrated radii as tetramethylammonium (TMA), tetraethylammonium (TEA), and tetrabutylammonium (TBA) ions. Even though tetraalkylammonium cations have hydrophobic constituents, note that there are experimental data suggesting

that water molecules around them can form hydration shells,[48−50] which is the so-called hydrophobic hydration effect.[51,52] These hydration shells may prevent the direct contact of hydrophobic cations with charged surfaces. In particular, Yakamata and Osawa have shown using infrared spectra that the hydration shells are tightly attached to these tetraalkylammonium ions and that large electric fields are required to destroy the corresponding hydration shells.[53,54] In addition, Inabe *et al.* have shown that large hydrated TBA cations are not tightly bound to negatively charged polar heads of mercaptoundecanoic acid (MUA) ligands.[55] This is consistent with the hydrophilic character of charged OH polar heads of MUA ligands[56] and with a weak electrostatic attraction between polar heads and TBA cations due to their large hydrated size. These experimental data suggest that short-range nonelectrostatic attractions between hydrated tetraalkylammonium cations and hydrophilic anionic nanoparticles should be negligible in the absence of specific interactions.

The total effective interaction potential between the nanoparticles is the sum of the corresponding electrostatic, repulsive-core, and van der Waals forces:

$$V(r) = V_{el}(r) + V_{rc}(r) + V_H(r) \quad (1)$$

where r is the center-to-center separation distance between the two nanoparticles, as displayed in the inset of Figure 2.

The components $V_{el}(r)$ and $V_{rc}(r)$ are calculated directly by integrating numerically, from infinite up to a position r, the total electrostatic and repulsive-core forces exerted on each nanoparticle:

$$V_{xx}(r) = \int_r^\infty F_{xx}(r)\, dr \quad (2)$$

where xx stands for el or rc. The difference in the dielectric properties of anionic nanoparticles and the aqueous solvent produces polarization effects that can be neglected in the presence of the monovalent ions and the high surface charge density of the colloids studied here (see the Supporting Information (SI) for further details). Thus, the total electrostatic force over each nanoparticle is determined by adding all the electrostatic pairwise forces coming from the Coulombic pair potentials:

$$\beta u_{ij}^{el}(r) = \frac{l_b}{r} z_i z_j \quad (3)$$

where z_i and z_j are the valences associated with particles of species i and j, respectively. In this definition, $\beta \equiv (k_B T)^{-1}$, where k_B is the Boltzmann constant and T is the temperature of the system, $l_b = e^2/(4\pi\varepsilon_0\varepsilon k_B T)$ is the corresponding Bjerrum length, ε_0 is the vacuum permittivity, and ε is the dielectric constant of the background medium. The total repulsive-core force over each nanoparticle, on the other hand, is calculated by adding all forces associated with the repulsive-core pair potential between a particle of species i and a particle of species j,

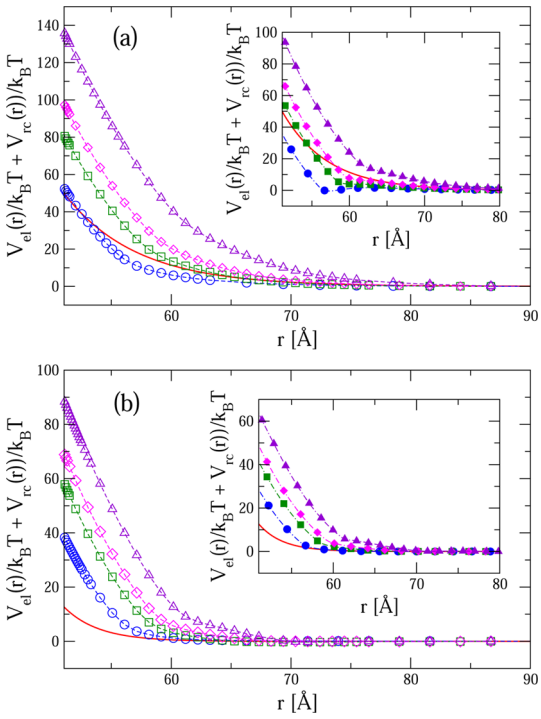

Figure 1. Electrostatic plus repulsive-core component of the potential of mean force between two anionic nanoparticles immersed in a 0.2 M (a) and a 1 M (b) monovalent electrolyte. Empty symbols correspond to simulation results and filled symbols to liquid theory calculations using the HNC approximation. Circles, squares, diamonds, and triangles are associated with NaOH, TMAOH, TEAOH, and TBAOH, respectively. The solid line is the potential of mean force according to the DLVO theory.

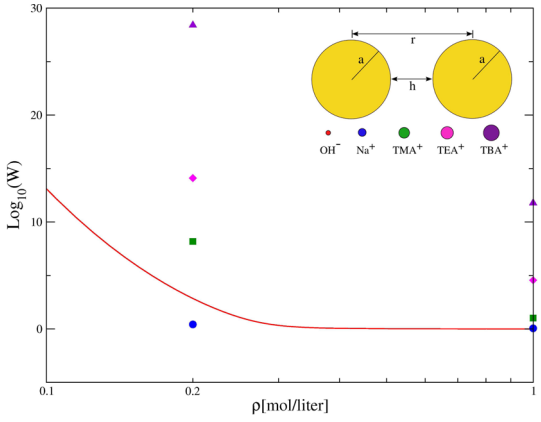

Figure 2. Stability ratio W that characterizes the colloidal stability of anionic nanoparticles as a function of the electrolyte concentration. Circles, squares, diamonds, and triangles correspond to simulation results using NaOH, TMAOH, TEAOH, and TBAOH, respectively. The solid line is the DLVO prediction.

separated by a distance r, which is modeled as follows: a hard core $u_{ij}^{rc}(r) = \infty$ for $r \leq \Delta_{ij}$, a shifted-truncated Lennard-Jones potential

$$\beta u_{ij}^{rc}(r) = 4\left[\left(\frac{\sigma}{r-\Delta_{ij}}\right)^{12} - \left(\frac{\sigma}{r-\Delta_{ij}}\right)^{6}\right] + 1 \quad (4)$$

for $\Delta_{ij} < r < \Delta_{ij} + 2^{1/6}\sigma$, and $u_{ij}^{rc}(r) = 0$ for $r \geq \Delta_{ij} + 2^{1/6}\sigma$, where $\Delta_{ij} = (d_i + d_j)/2 - \sigma$ is the hard-core diameter. The parameter σ regulates the hardness of the repulsive-core interactions. In order to mimic the hard core interaction characteristic of the primitive model, σ was set equal to 0.1 nm.

The electrostatic and repulsive-core components of the effective potential between two nanoparticles (corresponding to several electrolyte concentrations) are then calculated from molecular dynamics (MD) simulations[57,58] following the procedure described above. This study is complemented with similar calculations based on the results obtained from the hypernetted chain (HNC) closure[34,59,60] for the integral equation theory (see the SI for further details).

The attractive (van der Waals) interaction between the two anionic nanoparticles is modeled here as

$$V_H(r) = -\frac{A_H}{6}\left[\frac{2a^2}{4ah+h^2}+\frac{2a^2}{(2a+h)^2}+\ln\left(\frac{4ah+h^2}{(2a+h)^2}\right)\right] \quad (5)$$

where $a = d_M/2$ is the radius of the nanoparticle, $h = (r - 2a)$ (see inset in Figure 2), and $A_H = 3.25 \times 10^{-19} J$ is an effective Hamaker constant. The numerical value of this constant is consistent with the experimental colloidal stability of highly charged mercaptoundecanoic acid-capped gold nanoparticles in the presence of high concentrations of NaOH[37] (see also the SI for further details).

The implementation of the dressed ion theory[38] techniques to the analysis of the effective interaction among spherical macroions immersed in a supporting electrolyte of small spherical ions predicts that this interaction can always be written, when the concentration of such electrolyte is sufficiently low, as the sum of a short-range term plus a long-range term with the form of a screened electrostatic (Yukawa) potential:[39,40]

$$\beta V(r) = \beta V^*(r) + \frac{l_b}{E^{(se)}}\frac{\exp(-\eta r)}{r} A_M{}^2 \quad (6)$$

where $E^{(se)}$, η^{-1}, and A_M are, respectively, the corresponding effective permittivity, screening length, and renormalized macroion charge. In the limit of infinite macroion dilution, these parameters are directly determined from the correlations among the small ions in the bulk and their distribution around a single macroion. Thus, computer simulations for these conditions were also implemented in order to extract the corresponding values of these parameters for a representative subset of scenarios, following a procedure based on the general ideas of Ulander and Kjellander.[61]

Indeed, the electrostatic component of the DLVO potential, which is obtained from the linearized version of the mean field PB equation, also fits the form given by the Yukawa term in eq 6. Since the PB equation considers only point ions (thus neglecting ion correlations and excluded volume effects), the resulting values for the effective permittivity and screening length are given by $E^{(se)} = 1$ and $\eta = \kappa_D$, respectively, where the Debye length $\kappa_D{}^{-1}$ is defined by

$$\kappa_D{}^2 = 4\pi l_b \sum_i \rho_i z_i{}^2 \quad (7)$$

In this last relation, ρ_i and z_i are, respectively, the corresponding bulk densities and valences of the point ions, which in our case correspond to the monovalent cations and anions in the supporting electrolyte. From the assumption of infinite macroion dilution and the linearization of the PB equation, on the other hand, comes the form

$$A_M^{DLVO} = \frac{\exp(\kappa_D d_M/2)}{1+\kappa_D d_M/2} z_M \quad (8)$$

for the renormalized macroion charge. The standard DLVO potential is then completed by considering that $V^*(r)$ is given by the hard sphere potential $V_{HS}(r) = \infty$ if $r < d_M$ and zero otherwise,[7] plus a short-range van der Waals attraction that, in our case, is taken to be identical to the interaction in eq 5 to produce a comparable model whose results can be contrasted to the results obtained from the computer simulations.

The attractive and repulsive interactions among colloids in solution determine the corresponding coagulation rates or, alternatively, the stability of the colloidal dispersion. In the von Smoluchowski kinetics, the coagulation of colloidal particles is determined by the number of collisions between particles and aggregates assuming that two colloids cannot separate after a collision. If only short-range attractions are present, the number of collisions is determined by random Brownian motion. In such a scenario, it is possible to observe a *rapid* coagulation because there are no energy barriers preventing the contact between colliding particles. When energy barriers are present, the collision rate can be reduced significantly, yielding a *slow* coagulation.[62,63]

In the presence of short-range van der Waals attractions, $V_H(r)$, and hydrodynamic interactions, the steady-state flux of equally sized single colloids toward a central colloid that is also diffusing in Brownian motion can be written as[64,65]

$$J_0 = \frac{8\pi c_0 D_0 a}{\int_0^\infty \frac{\gamma(u)}{(u+2)^2}\exp(\beta V_H(u))\,du} \quad (9)$$

where

$$\gamma(u) = \frac{6u^2+13u+2}{6u^2+4u} \quad (10)$$

D_0 is the diffusion coefficient of a colloidal particle at infinite dilution, c_0 is the number of colloidal particles per unit volume, a is the radius of the colloidal particle,

and $u = (r - 2a)/a$. Note that, in general, the viscous drag experienced by two colloidal particles is not independent of their separation distance due to hydrodynamic interactions. A correction proposed by Honig *et al*. is included specifically *via* eq 10.

The coagulation rate between colliding charged colloids could be greatly reduced if the electrostatic repulsion due to the overlapping of the electrical double layers is significant. In this situation, it is possible to compare the corresponding rate of slow coagulation with that of rapid coagulation *via* the stability ratio W defined as[64,65]

$$W = \frac{J_0}{J} = \frac{\int_0^\infty \frac{\gamma(u)}{(u+2)^2} \exp(\beta V(u))\, du}{\int_0^\infty \frac{\gamma(u)}{(u+2)^2} \exp(\beta V_H(u))\, du} \qquad (11)$$

with $u = (r - 2a)/a$. In this definition, the effective pair potential used to describe the rapid coagulation is given by the short-range attractive interaction $V_H(r)$ (see eq 5). In the slow coagulation case, the effective pair potential, $V(r)$ (see eq 1), includes the electrostatic and repulsive-core effective interactions in addition to the short-range attractive potential $V_H(r)$. The rapid and slow coagulation rates can be measured experimentally using optical techniques.[66−68]

In this study, the colloidal stability can be characterized by incorporating the effective pair potentials $V(r)$ obtained from the MD simulations and those obtained from the DLVO theory described above into the stability ratio W. According to the definition given in eq 11, a value of the stability ratio W close to 1 indicates flocculation, when the van der Waals potential overcomes the repulsive effective interactions. Contrastingly, large values of the stability ratio W indicate that the repulsive energy barriers decrease significantly the collision rate between charged colloids, maintaining the colloidal suspension stable. The DLVO model is employed here in a straightforward fashion, without any attempt to include nonlinear effects by using effective charges nor to improve it by adding short-range contributions from the overlapping of the condensation layers. As shown below, this model then predicts highly screened electrostatic colloidal repulsions, which in turn yield a stability ratio $W \approx 1$ at high enough electrolyte concentrations. Our simulation results for $V(r)$, on the other hand, which include ion correlations and excluded volume effects, describe a more complex picture for the colloidal stability.

RESULTS AND DISCUSSION

The effects of the ionic size asymmetry in the sum of the electrostatic and repulsive-core components of the potential of mean force are displayed in Figure 1. Several monovalent salts with the same anion but different cation size (*i.e*., NaOH, TMAOH, TEAOH, and TBAOH) were considered at two distinct electrolyte concentrations (the physical parameters used in the simulation and theoretical calculations are given in Table 1). Here, we observe a strong repulsion between the anionic nanoparticles that augments significantly as a function of the ionic size of the cations. At the largest electrolyte concentration the electrostatic screening increases; nevertheless the repulsion due to electrostatic and repulsive-core interactions is still important for large cations.

TABLE 1. Parameter Values Used in the MD Simulations and the Integral Equation Approach[a]

valence of each nanoparticle	$z_M = -90$
valence of cations	$z_+ = +1$
valence of anions	$z_- = -1$
diameter of each nanoparticle	$d_M = 5.1$ nm
diameter of OH^-	$d_{OH} = 0.3$ nm
diameter of Na^+	$d_{Na} = 0.5$ nm
diameter of TMA^+	$d_{TMA} = 0.7$ nm
diameter of TEA^+	$d_{TEA} = 0.8$ nm
diameter of TBA^+	$d_{TBA} = 1.0$ nm
dielectric constant	$\varepsilon = 78.5$
temperature	$T = 298$ K
Bjerrum length	$l_b = 0.714$ nm

[a] Ionic sizes of OH^-, Na^+, TMA^+ (tetramethylammonium), TEA^+ (tetraethylammonium), and TBA^+ (tetrabutylammonium) were taken from refs 73−75.

The role of short-range interactions between the anionic nanoparticles in the stability ratio W is displayed in Figure 2. In this figure we observe that, according to our simulation results, anionic nanoparticles coagulate for concentrations greater than 0.2 M in the presence of the electrolyte with the smallest counterions (NaOH). In contrast, the logarithm of the stability ratio, $\log_{10}(W)$, is different from zero up to a 1 M concentration for the electrolytes with larger counterions. Experimental researchers are usually limited technically to measure stability ratios near the critical concentration of coagulation. However, since 1954 it has been possible to measure experimentally $\log_{10}(W)$ values as large as 5−6[69] (or W values between 10^5 and 10^6). Additionally, experimental values of $\log_{10}(W)$ larger than 2 also have been reported in many colloidal science textbooks and research articles.[7,62,70,71] According to our simulation data displayed in Figure 2, the value of $\log_{10}(W)$ is approximately 0, 1, 4.6, and 11.8 for Na, TMA, TEA, and TBA cations, respectively, at the highest salt concentration. Although a large $\log_{10}(W)$ value is associated with the electrolyte with the largest cation, notice that the stability ratios of the other cations are measurable experimentally.[7,62,69−71] The nonzero values of $\log_{10}(W)$ suggest that the corresponding colloidal solution should be stable, as it has been observed indeed experimentally at analogous conditions.[37] Even though the stability ratio was not measured experimentally in that work,[37] it was observed that an aqueous solution of highly charged anionic nanoparticles coagulated at high electrolyte concentrations of NaOH, whereas the colloidal suspension

remained stable in the presence of larger counterions at salt concentrations as high as 1 M. This behavior is consistent with the simulation data displayed in Figure 2. It is also worthwhile mentioning that even though the DLVO theory displays a behavior similar to that shown by the salt with the smallest counterions (NaOH) at high ionic concentrations, it deviates significantly for lower electrolyte concentrations at the same surface charge density if charge regulation effects are neglected (not shown). This means that the DLVO theory grossly overestimates the electrostatic repulsion between highly charged nanoparticles, as previously reckoned.[72]

The total effective interaction potentials obtained *via* MD simulations at a 0.2 M concentration are plotted in Figure 3a. It is clear here that the interaction between the nanoparticles in the presence of the electrolyte with the smallest counterions (NaOH) is mainly attractive. Interestingly, the DLVO theory predicts a larger repulsion than is observed in the presence of the NaOH salt. In contrast, simulation results for the total interaction potential in the presence of larger counterions show a more repulsive interaction that increases its strength as a function of the ionic size of counterions (*i.e.*, TMA, TEA, and TBA cations). A repulsive maximum displayed by large counterions, absent in the NaOH instance, thus enhances the colloidal stability of anionic nanoparticles. In the inset of Figure 3a we also display theoretical predictions based on the HNC approximation, which also includes ion correlations and excluded volume effects. The HNC theory agrees in general with the simulation results, though it seems to underestimate the electrostatic and repulsive-core interactions.

The total effective interaction potentials at a 1 M concentration are plotted in Figure 3b. In this instance, we observe that for the salt with the smallest counterions (as for the DLVO theory) the interaction potential is negative for all separations of the nanoparticles, which explains why the nanoparticles coagulate in this regime. In contrast, simulation and HNC results still display short-range repulsive interactions for larger counterions, thus increasing the colloidal stability of highly charged nanoparticles at high electrolyte concentrations.

We can gain a deeper understanding of the origin of the previous observations by analyzing the behavior of the electrostatic ($V_{el}(r)$) and repulsive-core ($V_{rc}(r)$) components of the interaction potential, which are reported in Figure 4 for the cases corresponding to the largest and smallest counterion sizes considered here, at a concentration of 1 M. As we observe, the repulsive-core interaction for the salt with the smallest counterions (NaOH) is approximately three times larger than the corresponding electrostatic repulsion at contact, attesting that excluded volume and entropic effects are quite important in this regime. Nevertheless, the

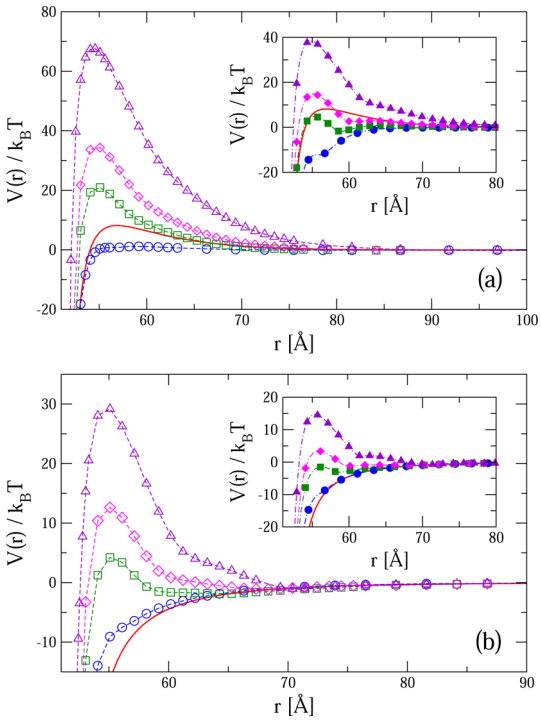

Figure 3. Potential of mean force between two anionic nanoparticles immersed in a 0.2 M (a) and a 1 M (b) monovalent electrolyte. Empty symbols correspond to simulation results, and filled symbols to liquid theory calculations using the HNC approximation. Circles, squares, diamonds, and triangles are associated with NaOH, TMAOH, TEAOH, and TBAOH, respectively. The solid line is the potential of mean force according to the DLVO theory.

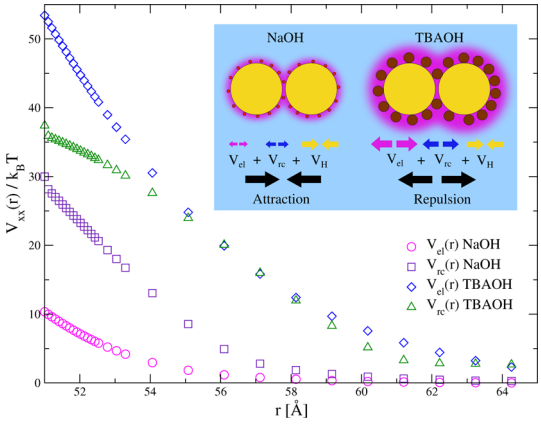

Figure 4. Electrostatic ($V_{el}(r)$) and repulsive-core ($V_{rc}(r)$) interaction potentials as a function of the distance between two anionic nanoparticles in the presence of 1 M NaOH and 1 M TBAOH obtained *via* MD simulations.

net sum of these two components is not repulsive enough in this case to overcome the van der Waals attraction, as established in Figure 3b. In contrast, the presence of the largest counterions (TBAOH) induces an electrostatic repulsion near the contact that is five times stronger than that displayed for the electrolyte with the smallest counterions (NaOH). Thus, the enhanced colloidal stability in the presence of large counterions and small co-ions is promoted mainly by a

thicker Stern-like (condensation) layer that shields the bare charge of the nanoparticles less efficiently than in the case of smaller counterions at high surface charge densities. In addition, the repulsive-core contribution becomes stronger as the size of counterions increases. The overall effect is the appearance of the repulsive peak already shown in Figure 3b, which reflects the fact that the electrostatic and repulsive-core contributions surpass the van der Waals attraction for larger counterions. This mechanism for preventing charged colloids from aggregating at high electrolyte concentrations is summarized in the scheme displayed in the inset of Figure 4. In addition, since our monovalent ions are all hydrophilic, this mechanism is complementary to the adsorption of large hydrophobic anions to hydrophobic anionic particles, which makes the charged suspension more stable.[17] It is worth mentioning here that even though $V_{el}(r)$ and $V_{rc}(r)$ have been plotted as two different curves, the electrostatic and excluded volume effects they describe are coupled in a nontrivial manner, as it has been extensively discussed for the primitive model.[76,77]

Further insight into the nature of the enhanced electrostatic repulsion can be attained by looking also at the effective parameters of the screened electrostatic component of the macroion−macroion potential, defined by eq 6. As mentioned above, the values for these parameters are directly obtained from complementary MD simulations of the electrolyte in the bulk and around a single charged nanoparticle. For the model system under consideration, it is found that the functional form of eq 6 ceases to be valid for the 1 M electrolyte concentration (at which point the system finds itself near or above the κ-transition[61]), so only lower concentrations are discussed here. For all the cases under consideration the effective permittivity $E^{(se)} \approx 1$, and consequently the relevant parameters are the inverse screening length η and the renormalized charge A_M. In Figure 5 are plotted, for several salt concentrations, the ratio A_M/A_M^{DLVO} for the four counterion sizes considered (main panel), where A_M^{DLVO} is defined in eq 8, and the ratio η/κ_D for the cases with the smallest (NaOH) and the largest (TBAOH) counterions (inset). The first thing to notice is that both ratios increase with increasing electrolyte concentration, and this is more noticeable when the counterion size is larger. The results for η/κ_D show clearly that the Debye length becomes less reliable as an approximation for the screening length when the electrolyte concentration rises,[38,61] but the size of the counterion seems to be of rather minor consequence. The results for the renormalized charge, on the other hand, show the huge impact that the counterion size has on this parameter and how this effect is magnified when the concentration grows. At the lowest ionic strength discussed here, the values of A_M corresponding to the four counterion sizes are almost identical and about

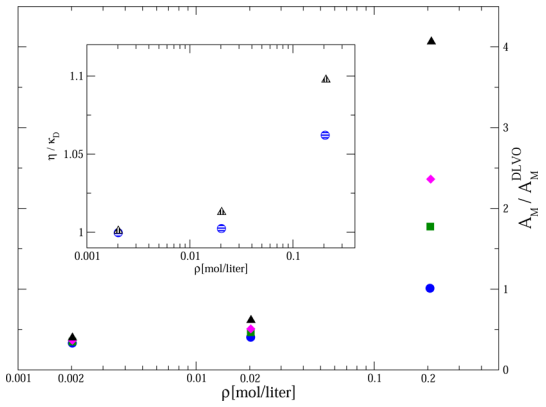

Figure 5. Ratio of the long-range renormalized charge A_M with respect to the corresponding DLVO renormalized charge A_M^{DLVO} (main panel) and ratio of the inverse screening length η with respect to the inverse Debye length κ_D (inset), as a function of the electrolyte concentration. Circles, squares, rhombuses, and triangles correspond to simulation results using NaOH, TMAOH, TEAOH, and TBAOH, respectively.

one-half of the DLVO value. In contrast, for the highest salt concentration presented in this figure, we have a much larger dispersion in the values of the renormalized charge, starting with $A_M \approx A_M^{DLVO}$ for NaOH and reaching up to $A_M \approx 4A_M^{DLVO}$ for TBAOH. This trend reinforces the stability of the suspended nanoparticles against flocculation induced by the enhanced short-range repulsions prompted by the larger counterions.

CONCLUDING REMARKS

We have shown here that ion correlations and excluded volume effects can enhance the colloidal stability of highly charged anionic nanoparticles in the presence of large counterions at high electrolyte concentrations. These results, obtained from detailed computer simulations and standard liquid theory approaches, are in line with experimental results of colloidal stability of highly charged anionic nanoparticles.[37] On the other hand, the stability ratio W predicted by the DLVO theory at high electrolyte concentrations displays a good agreement with simulation results for the salt with the smallest cation (NaOH).

The origin of the enhanced colloidal stability promoted by large counterions and small co-ions can be understood in terms of increased short-range electrostatic and steric repulsions arising from a swollen Stern-like layer at high surface charge densities of the nanoparticles. These effects are certainly not taken into account in the classical PB theory. Furthermore, even the integral equation HNC approach fails to account for the full scope of this repulsive strengthening, especially at concentrations below 0.2 M, where an incorrectly large attraction is predicted, and lack of convergence is eventually reached for sufficiently dilute systems. Thus, a proper description of the repulsive enhancements discussed here poses a theoretical challenge that might perhaps be overcome with more

sophisticated approaches, based on modified PB theories,[78] density functional approaches,[79−82] or improved integral equation schemes.[83−87]

In addition, we have demonstrated that increasing the counterion size augments the renormalized charge that regulates the long-range interaction among macroions, an effect that is clearly more important as the ionic concentration rises. This amplification of the renormalized charge, due to the less efficient shielding of the bare macroion charge by large counterions, should be detectable in experiments that directly measure the net interaction between two macroions at sufficiently large separation distances.[88] Furthermore, this enhanced long-range repulsion complements the increased short-range repulsion induced by larger counterions, thus boosting the stability of suspensions of highly charged nanoparticles in concentrated electrolyte solutions.

MATERIALS AND METHODS

Molecular Dynamics Simulations. Two identical nanoparticles were located at fixed positions along one diagonal of a cubic simulation box, symmetrically placed with respect to the center of the cell, under periodic boundary conditions. Size-asymmetric monovalent ions free to move were also placed inside the simulation box. The charged particles fulfilled the electroneutrality condition:

$$2z_M + z_c N_c + z_+ N_+ + z_- N_- = 0 \qquad (12)$$

where N_+ and N_- are, respectively, the number of bulk monovalent cations and anions, while z_c and N_c are the corresponding valence and number of monovalent counterions (which are in this case identical to the cations) added to compensate the charge of the two nanoparticles. The MD simulations were performed using the LAMMPS package[57,58] in the NVT ensemble *via* a Nosé−Hoover thermostat[89,90] at a reduced temperature $T' = k_B T/\varepsilon = 1$, where $\varepsilon = k_B T$ is the thermal energy. The time step used was 0.04τ, where τ is the reduced Lennard-Jones unit of time. Long-range Coulombic interactions were handled properly using Ewald sums. The total number of ions, $N = N_+ + N_- + N_c$, used in simulations ranged from 3000 to 8000. Between 1 and 6 million MD time steps were used to thermalize the system. The total repulsive-core and electrostatic forces acting over each nanoparticle were sampled each 10 MD time steps (in a compromise between efficiency and reduction of time correlations), and between 26 and 52 million MD time steps were performed to calculate the time average of the forces. Mean force curves for several positions were generated for each electrolyte and then integrated to obtain the corresponding potentials of mean force.

Complementary MD simulations of the electrolyte in bulk and around one single charged nanoparticle were also performed following a protocol similar to that described above. The corresponding radial distribution functions were then used to determine the asymptotic behavior of the total correlation functions.

Screened Coulomb Parameters from Computer Simulations. The Ornstein−Zernike (OZ) equations

$$h_{mn}(r_{12}) = c_{mn}(r_{12}) + \sum_p \rho_p \int d\vec{r}_3 c_{mp}(r_{13}) h_{pn}(r_{32}) \qquad (13)$$

define the direct correlation functions $c_{mn}(r)$ in terms of the total correlation functions $h_{mn}(r) \equiv g_{mn}(r) - 1$. For charged systems, each direct correlation function takes the form $c_{mn}(r) = c^s_{mn}(r) - l_b z_m z_n / r$, where the term $c^s_{mn}(r)$ is the corresponding short-range component. The main result of the dressed ion theory is that, for sufficiently dilute solutions, the asymptotic behavior of $h_{mn}(r)$ is necessarily of the form $h_{mn}(r) \approx -l_b \exp(-\kappa r) z^*_m z^*_n / E^* r$, where κ is the global screening length, E^* is the effective permittivity, and z^*_m is the renormalized charge of species m.[38] These parameters are determined by the full set of functions $\tilde{c}^s_{mn}(k)$, which can be garnered from the MD data following the general ideas proposed by Ulander and Kjellander.[61] In our implementation of this approach the distribution functions obtained from the simulations, $g^{sim}_{ij}(r)$, are used as the core input for an *ad hoc* set of closures defined by $g_{ij}(r) = g^{sim}_{ij}(r)$ for $r \le R^c_{ij}$ and $g_{ij}(r) = \exp(\xi^s_{ij}(r) - \beta u^{rc}_{ij}(r))$ for $r > R^c_{ij}$, where $\xi^s_{ij}(r) = h_{ij}(r) - c^s_{ij}(r)$ and R^c_{ij} are, respectively, the corresponding indirect correlation functions and cutoff distances. In the second part of our closure, the affiliated bridge functions have been neglected. By choosing sufficiently large cutoff distances, we make sure that the implicit bridge functions become indeed negligible beyond those distances,[91] so the ensuing error in the estimated parameters turns out to be less than 5% (see the SI for further details). In the limit of infinite nanoparticle dilution considered here (*i.e.*, $\rho_M = 0$), the effective pair potential between macroions is given by $\beta V(r) = -\ln(g_{MM}(r))$. Consequently $\eta = \kappa$, $E^{(se)} = E^*$, and $A_M = z^*_M$.

Conflict of Interest: The authors declare no competing financial interest.The authors declare no competing financial interest.

Supporting Information Available: Details about the hypernetted chain approximation, the asymptotic behavior of the total correlation functions, the effects of the dielectric discontinuity, and the numerical value of the effective Hamaker constant are provided. This material is available free of charge via the Internet at http://pubs.acs.org.

Acknowledgment. We thank Luc Belloni for valuable discussions and insightful suggestions, Yan Levin for useful comments, Gabriel Longo for valuable discussions, and the Quest computer cluster at Northwestern University for the computing time provided. G.I.G.G. thanks the support of the NSF MRSEC award No. DMR-1121262, and P.G.M. and M.O.C. thank the support of the AFOSR Award FA9550-10-1-0167.

REFERENCES AND NOTES

1. Hainfeld, J. F.; Powell, R. D.; Hacker, G. W. *Nanoparticle Molecular Labels. Nanobiotechnology: Concepts, Applications and Perspectives*; Niemeyer, C. M.; Mirkin, C. A., Eds.; Wiley-VCH: Weinheim, 2004; pp 353−386.
2. Glomm, W. R. Functionalized Gold Nanoparticles for Applications in Bionanotechnology. *J. Dispersion Sci. Technol.* **2005**, *26*, 389–414.
3. Hühn, D.; Kantner, K.; Geidel, C.; Brandholt, S.; De Cock, I.; Soenen, S. J. H.; Rivera Gil, P.; Montenegro Martos, J. M.; Braeckmans, K.; Müllen, K.; *et al.* Polymer-Coated Nanoparticles Interacting with Proteins and Cells: Focusing on the Sign of the Net Charge. *ACS Nano* **2013**, *7*, 3253–3263.
4. Rivera Gil, P.; Jimenez de Aberasturi, D.; Wulf, V.; Pelaz, B.; del Pino, P.; Zhao, Y.; de la Fuente, J.; Ruiz de Larramendi, I.; Rojo, T.; Liang, X.-J. The Challenge to Relate the Physicochemical Properties of Colloidal Nanoparticles to Their Cytotoxicity. *Acc. Chem. Res.* **2013**, *46*, 743–749.
5. Chanana, M.; Rivera Gil, P.; Correa-Duarte, M. A.; Liz-Marzán, L. M.; Parak, W. J. Physicochemical Properties of Protein-Coated Gold Nanoparticles in Biological Fluids and Cells before and after Proteolytic Digestion. *Angew. Chem., Int. Ed.* **2013**, *52*, 4179–4183.
6. Verwey, E. J. W.; Overbeek, J. T. G. *Theory of the Stability of Lyophobic Colloids*; Elsevier: New York, 1948.
7. Russel, W. B.; Saville, D. A.; Schowalter, W. R. *Colloidal Dispersions*; Cambridge University Press: Cambridge, 1989.
8. Medina-Noyola, M.; McQuarrie, D. A. On the Interaction of Spherical Double Layers. *J. Chem. Phys.* **1980**, *73*, 6279–6283.

9. Kjellander, R.; Marčelja, S. Double-Layer Interaction in the Primitive Model and the Corresponding Poisson-Boltzmann Description. *J. Phys. Chem.* **1986**, *90*, 1230–1232.
10. Kjellander, R.; Marčelja, S. Interaction of Charged Surfaces in Electrolyte Solutions. *Chem. Phys. Lett.* **1986**, *127*, 402–407.
11. Raspaud, E.; Olvera de la Cruz, M.; Sikorav, J. L.; Livolant, F. Precipitation of DNA by Polyamines: A Polyelectrolyte Behavior. *Biophys. J.* **1998**, *74*, 381–393.
12. Rodgers, J. M.; Kaur, C.; Chen, Y. G.; Weeks, J. D. Attraction between Like-Charged Walls: Short-Ranged Simulations Using Local Molecular Field Theory. *Phys. Rev. Lett.* **2006**, *97*, 097801.
13. Quesada-Pérez, M.; González-Tovar, E.; Martín-Molina, A.; Lozada-Cassou, M.; Hidalgo-Álvarez, R. Ion Size Correlations and Charge Reversal in Real Colloids. *Colloids Surf., A* **2005**, *267*, 24–30.
14. Bratko, D.; Jönsson, B.; Wennerström, H. Electrical Double Layer Interactions with Image Charges. *Chem. Phys. Lett.* **1986**, *128*, 449–454.
15. Wang, Z.-Y.; Ma, Y.-Q. Monte Carlo Determination of Mixed Electrolytes next to a Planar Dielectric Interface with Different Surface Charge Distributions. *J. Chem. Phys.* **2009**, *131*, 244715.
16. Bakhshandeh, A.; dos Santos, A. P.; Levin, Y. Weak and Strong Coupling Theories for Polarizable Colloids and Nanoparticles. *Phys. Rev. Lett.* **2011**, *107*, 107801.
17. dos Santos, A. P.; Levin, Y. Ion Specificity and the Theory of Stability of Colloidal Suspensions. *Phys. Rev. Lett.* **2011**, *106*, 167801.
18. Alexander, S.; Chaikin, P. M.; Grant, P.; Morales, G. J.; Pincus, P.; Hone, D. Charge Renormalization, Osmotic Pressure, and Bulk Modulus of Colloidal Crystals: Theory. *J. Chem. Phys.* **1984**, *80*, 5776–5781.
19. Belloni, L.; Drifford, M.; Turq, P. Counterion Diffusion in Polyelectrolyte Solutions. *Chem. Phys.* **1984**, *83*, 147–154.
20. Belloni, L. Ionic Condensation and Charge Renormalization in Colloidal Suspensions. *Colloids Surf., A* **1998**, *140*, 227–243.
21. Colla, T. E.; Levin, Y.; Trizac, E. A Self-Consistent Renormalized Jellium Approach for Calculating Structural and Thermodynamic Properties of Charge Stabilized Colloidal Suspensions. *J. Chem. Phys.* **2009**, *131*, 074115.
22. Denton, A. R. Poisson-Boltzmann Theory of Charged Colloids: Limits of the Cell Model for Salty Suspensions. *J. Phys.: Condens. Matter* **2010**, *22*, 364108.
23. Falcón-González, J. M.; Castañeda-Priego, R. Note: Renormalized Jellium Model for Charged Colloids Revisited. *J. Chem. Phys.* **2010**, *133*, 216101.
24. Olvera de la Cruz, M.; Belloni, L.; Delsanti, M.; Dalbiez, J. P.; Spalla, O.; Drifford, M. Precipitation of Highly Charged Polyelectrolyte Solutions in the Presence of Multivalent Salts. *J. Chem. Phys.* **1995**, *103*, 5781–5791.
25. Solis, F. J.; Olvera de la Cruz, M. Collapse of Flexible Polyelectrolytes in Multivalent Salt Solutions. *J. Chem. Phys.* **2000**, *112*, 2030–2035.
26. Solis, F. J.; Olvera de la Cruz, M. Flexible Linear Polyelectrolytes in Multivalent Salt Solutions: Solubility Conditions. *Eur. Phys. J. E: Soft Matter Biol. Phys.* **2001**, *4*, 143–152.
27. Widom, J.; Baldwin, R. L. Cation-Induced Toroidal Condensation of DNA Studies with $Co^{3+}(NH_3)_6$. *J. Mol. Biol.* **1980**, *144*, 431–453.
28. Zhang, F.; Skoda, M. W. A.; Jacobs, R. M. J.; Zorn, S.; Martin, R. A.; Martin, C. M.; Clark, G. F.; Weggler, S.; Hildebrandt, A.; Kohlbacher, O.; *et al.* Reentrant Condensation of Proteins in Solution Induced by Multivalent Counterions. *Phys. Rev. Lett.* **2008**, *101*, 148101.
29. Solis, F. J. Phase Diagram of Dilute Polyelectrolytes: Collapse and Redissolution by Association of Counterions and Co-ions. *J. Chem. Phys.* **2002**, *117*, 9009–9015.
30. Hsiao, P. Y.; Luijten, E. Salt-Induced Collapse and Reexpansion of Highly Charged Flexible Polyelectrolytes. *Phys. Rev. Lett.* **2006**, *97*, 148301.
31. Aranda-Espinoza, H.; Chen, Y.; Dan, N.; Lubensky, T. C.; Nelson, P.; Ramos, L.; Weitz, D. A. Electrostatic Repulsion of Positively Charged Vesicles and Negatively Charged Objects. *Science* **1999**, *285*, 394–397.
32. Gomez, E. W.; Clack, N. G.; Wu, H. J.; Groves, J. T. Like-Charge Interactions between Colloidal Particles Are Asymmetric with Respect to Sign. *Soft Matter* **2009**, *5*, 1931–1936.
33. Kane, J.; Inan, M.; Saraf, R. F. Self-Assembled Nanoparticle Necklaces Network Showing Single-Electron Switching at Room Temperature and Biogating Current by Living Microorganisms. *ACS Nano* **2010**, *4*, 317–323.
34. Guerrero-García, G. I.; González-Mozuelos, P.; Olvera de la Cruz, M. Potential of Mean Force between Identical Charged Nanoparticles Immersed in a Size-Asymmetric Monovalent Electrolyte. *J. Chem. Phys.* **2011**, *135*, 164705.
35. Semenov, I.; Raafatnia, S.; Sega, M.; Lobaskin, V.; Holm, C.; Kremer, F. Electrophoretic Mobility and Charge Inversion of a Colloidal Particle Studied by Single-Colloid Electrophoresis and Molecular Dynamics Simulations. *Phys. Rev. E: Stat. Phys., Plasmas, Fluids, Relat. Interdiscip. Top.* **2013**, *87*, 022302.
36. Walker, D. A.; Kowalczyk, B.; Olvera de la Cruz, M.; Grzybowski, B. A. Electrostatics at the Nanoscale. *Nanoscale* **2011**, *3*, 1316–1344.
37. Laaksonen, T.; Ahonen, P.; Johans, C.; Kontturi, K. Stability and Electrostatics of Mercaptoundecanoic Acid-Capped Gold Nanoparticles with Varying Counterion Size. *ChemPhysChem* **2006**, *7*, 2143–2149.
38. Kjellander, R.; Mitchell, D. J. Dressed-Ion Theory for Electrolyte Solutions: A Debye-Hückel-Like Reformulation of the Exact Theory for the Primitive Model. *J. Chem. Phys.* **1994**, *101*, 603–626.
39. González-Mozuelos, P.; Carbajal-Tinoco, M. D. Effective Pair Potentials for Charged Colloidal Particles. *J. Chem. Phys.* **1998**, *109*, 11074–11084.
40. Carbajal-Tinoco, M. D.; González-Mozuelos, P. Effective Attractions between Like-Charged Colloidal Particles. *J. Chem. Phys.* **2002**, *117*, 2344–2350.
41. Tohver, V.; Smay, J. E.; Braem, A.; Braun, P. V.; Lewis, J. A. Nanoparticle Halos: A New Colloid Stabilization Mechanism. *Proc. Natl. Acad. Sci. U.S.A.* **2001**, *98*, 8950–8954.
42. Chávez-Páez, M.; González-Mozuelos, P.; Medina-Noyola, M.; Méndez-Alcaraz, J. M. Polyion Monolayers and Halos around Large Weakly-Charged Colloids. *Phys. A (Amsterdam, Neth.)* **2004**, *341*, 1–22.
43. Ji, S.; Herman, D.; Walz, J. Y. Manipulating Microparticle Interactions Using Highly Charged Nanoparticles. *Colloids Surf., A* **2012**, *396*, 51–62.
44. McKee, C. T.; Walz, J. Y Interaction Forces between Colloidal Particles in a Solution of Like-Charged, Adsorbing Nanoparticles. *J. Colloids Interface Sci.* **2012**, *365*, 72–80.
45. Xing, X.; Sun, G.; Li, Z.; Ngai, T. Stabilization of Colloidal Suspensions: Competing Effects of Nanoparticle Halos and Depletion Mechanism. *Langmuir* **2012**, *28*, 16022–16028.
46. Herman, D.; Walz, J. Y. Stabilization of Weakly Charged Microparticles Using Highly Charged Nanoparticles. *Langmuir* **2013**, *29*, 5982–5994.
47. Huang, H.; Ruckenstein, E. Decoration of Microparticles by Highly Charged Nanoparticles. *J. Phys. Chem. B* **2013**, *117*, 6318–6322.
48. Green, J. L.; Sceats, M. G.; Lacey, A. R. Hydrophobic Effects in the Water Network Structure of Aqueous Solutions of a Semiclathrate Molecule. *J. Chem. Phys.* **1987**, *87*, 3603–3610.
49. Turner, J.; Soper, A. K. The Effect of Apolar Solutes on Water Structure: Alcohols and Tetraalkylammonium Ions. *J. Chem. Phys.* **1994**, *101*, 6116–6125.
50. Stangret, J.; Gampe, T. Hydration Sphere of Tetrabutylammonium Cation. FTIR Studies of HDO Spectra. *J. Phys. Chem. B* **1999**, *103*, 3778–3783.
51. Wen, W.-Y. *Water and Aqueous Solutions*; Horne, R. A., Ed.; Wiley-Interscience: New York, 1972.
52. Blokzijl, W.; Engberts, J. B. F. N. Hydrophobic Effects. Opinions and Facts. *Angew. Chem., Int. Ed. Engl.* **1993**, *32*, 1545–1579.
53. Yamakata, A.; Osawa, M. Destruction of the Hydration Shell around Tetraalkylammonium Ions at the Electrochemical Interface. *J. Am. Chem. Soc.* **2009**, *131*, 6892–6893.

54. Yamakata, A.; Osawa, M. Destruction of the Water Layer on a Hydrophobic Surface Induced by the Forced Approach of Hydrophilic and Hydrophobic Cations. *J. Phys. Chem. Lett.* **2010**, *1*, 1487–1491.
55. Miyahira, T.; Hasegawa, H.; Takahashi, Y.; Inabe, T. Electrochemical Crystallization of Organic Molecular Conductors: Electrode Surface Conditions for Crystal Growth. *Cryst. Growth Des.* **2013**, *13*, 1955–1960.
56. Hiasa, T.; Kimura, K.; Onishi, H. Hydration of Hydrophilic Thiolate Monolayers Visualized by Atomic Force Microscopy. *Phys. Chem. Chem. Phys.* **2012**, *14*, 8419–8424.
57. Plimpton, S. Fast Parallel Algorithms for Short-Range Molecular Dynamics. *J. Comput. Phys.* **1995**, *117*, 1–19.
58. *LAMMPS Molecular Dynamics Simulator*; http://lammps.sandia.gov/ (August 20, 2010).
59. Cortada, M.; Anta, J. A.; Molina-Bolívar, J. A. Secondary Minimum Coagulation in Charged Colloidal Suspensions from Statistical Mechanics Methods. *J. Phys. Chem. B* **2007**, *111*, 1110–1118.
60. Moncho-Jordá, A.; Anta, J. A.; Callejas-Fernández, J. Effective Electrostatic Interactions Arising in Core-Shell Charged Microgel Suspensions with Added Salt. *J. Chem. Phys.* **2013**, *138*, 134902.
61. Ulander, J.; Kjellander, R. The Decay of Pair Correlation Functions in Ionic Fluids: A Dressed Ion Theory Analysis of Monte Carlo Simulations. *J. Chem. Phys.* **2001**, *114*, 4893–4904.
62. Hiemenz, P. C.; Rajagopalan, R. *Principles of Colloid and Surface Chemistry*; Marcel Dekker, Inc.: New York, 1997.
63. Wennerström, H.; Evans, D. F. *The Colloidal Domain: Where Physics, Chemistry, and Biology Meet*; Wiley-VCH: New York, 1999.
64. Honig, E. P.; Roebersen, G. J.; Wiersema, P. H. Effect of Hydrodynamic Interaction on the Coagulation Rate of Hydrophobic Colloids. *J. Colloid Interface Sci.* **1971**, *36*, 97–109.
65. Sonntag, H.; Strenge, K. *Coagulation Kinetics and Structure Formation*; Plenum Press: New York, 1987.
66. Kruyt, H. R., Ed. *Colloid Science*; Elsevier Publishing Company: New York, 1952.
67. Holthoff, H.; Egelhaaf, S. U.; Borkovec, M.; Schurtenberger, P.; Sticher, H. Coagulation Rate Measurements of Colloidal Particles by Simultaneous Static and Dynamic Light Scattering. *Langmuir* **1996**, *12*, 5541–5549.
68. Schneider, C.; Hanisch, M.; Wedel, B.; Jusufi, A.; Ballauff, M. Experimental Study of Electrostatically Stabilized Colloidal Particles: Colloidal Stability and Charge Reversal. *J. Colloid Interface Sci.* **2011**, *358*, 62–67.
69. Reerink, H.; Overbeek, J. T. G. The Rate of Coagulation as a Measure of the Stability of Silver Iodide Sols. *Discuss. Faraday Soc.* **1954**, *18*, 74–84.
70. Park, Y.; Franses, E. I. Effect of a PEGylated Lipid on the Dispersion Stability and Dynamic Surface Tension of Aqueous DPPC and on the Interactions with Albumin. *Langmuir* **2010**, *26*, 6932–6942.
71. Park, Y.; Huang, R.; Corti, D. S.; Franses, E. I. Colloidal Dispersion Stability of Unilamellar DPPC Vesicles in Aqueous Electrolyte Solutions and Comparisons to Predictions of the DLVO Theory. *J. Colloid Interface Sci.* **2010**, *342*, 300–310.
72. Colla, T. E.; dos Santos, A. P.; Levin, Y. Equation of State of Charged Colloidal Suspensions and Its Dependence on the Thermodynamic Route. *J. Chem. Phys.* **2012**, *136*, 194103.
73. Marcus, Y. Ionic Radii in Aqueous Solutions. *Chem. Rev. (Washington, DC, U. S.)* **1988**, *88*, 1475–1498.
74. Robinson, R. A.; Stokes, R. H. *Electrolyte Solutions*; Dover: London, 1959.
75. Coetzee, J. F.; Cunningham, G. P. Evaluation of Single Ion Conductivities in Acetonitrile, Nitromethane, and Nitrobenzene Using Tetraisoamylammonium Tetraisoamylboride as Reference Electrolyte. *J. Am. Chem. Soc.* **1965**, *87*, 2529–2534.
76. Kjellander, R. Intricate Coupling between Ion-Ion and Ion-Surface Correlations in Double Layers as Illustrated by Charge Inversion-Combined Effects of Strong Coulomb Correlations and Excluded Volume. *J. Phys.: Condens. Matter* **2009**, *21*, 424101.
77. Guerrero-García, G. I.; González-Tovar, E.; Olvera de la Cruz, M. Effects of the Ionic Size-Asymmetry around a Charged Nanoparticle: Unequal Charge Neutralization and Electrostatic Screening. *Soft Matter* **2010**, *6*, 2056–2065.
78. Bhuiyan, L. B.; Outhwaite, C. W.; Henderson, D. A Monte Carlo Study of the Structure of a Planar Electric Double Layer Containing Asymmetric Electrolytes. *J. Chem. Eng. Data* **2011**, *56*, 4556–4563.
79. Goel, T.; Patra, C. N.; Ghosh, S. K.; Mukherjee, T. Effect of Ionic Size on the Structure of Cylindrical Electric Double Layers: A Systematic Study by Monte Carlo Simulations and Density Functional Theory. *J. Phys. Chem. B* **2011**, *115*, 10903–10910.
80. Vibhu, I.; Modak, B.; Patra, C. N.; Ghosh, S. K. Zeta Potential of Colloidal Particle in Solvent Primitive Model Electrolyte Solution: A Density Functional Theory Study. *Mol. Phys.* **2013**, *111*, 489–496.
81. Frydel, D.; Levin, Y. A Close Look into the Excluded Volume Effects within a Double Layer. *J. Chem. Phys.* **2012**, *137*, 164703.
82. Borgis, D.; Gendre, L.; Ramirez, R. Molecular Density Functional Theory: Application to Solvation and Electron-Transfer Thermodynamics in Polar Solvents. *J. Phys. Chem. B* **2012**, *116*, 2504–2512.
83. Belloni, L. Colloid-Counterion Mixtures: An Advanced Integral Equation. *J. Phys.: Condens. Matter* **2002**, *14*, 9323–9337.
84. Marucho, M.; Kelley, C. T.; Pettitt, B. M. Solutions of the Optimized Closure Integral Equation Theory: Heteronuclear Polyatomic Fluids. *J. Chem. Theory Comput.* **2008**, *4*, 385–396.
85. Maruyama, Y.; Hirata, F. Modified Anderson Method for Accelerating 3D-RISM Calculations Using Graphics Processing Unit. *J. Chem. Theory Comput.* **2012**, *8*, 3015–3021.
86. Puibasset, J.; Belloni, L. Bridge Function for the Dipolar Fluid from Simulation. *J. Chem. Phys.* **2012**, *136*, 154503.
87. Zwanikken, J.; Olvera de la Cruz, M. Tunable Soft Structure in Charged Fluids Confined by Dielectric Interfaces. *Proc. Natl. Acad. Sci. U.S.A.* **2013**, *110*, 5301–5308.
88. Gutsche, C.; Keyser, U. F.; Kegler, K.; Kremer, F.; Linse, P. Forces between Single Pairs of Charged Colloids in Aqueous Salt Solutions. *Phys. Rev. E: Stat. Phys., Plasmas, Fluids, Relat. Interdiscip. Top.* **2007**, *76*, 031403.
89. Nosé, S. A Molecular Dynamics Method for Simulations in the Canonical Ensemble. *Mol. Phys.* **1984**, *52*, 255–268.
90. Hoover, W. G. Canonical Dynamics: Equilibrium Phase-Space Distributions. *Phys. Rev. A: At., Mol., Opt. Phys.* **1985**, *31*, 1695–1697.
91. González-Mozuelos, P.; Guerrero-García, G. I.; Olvera de la Cruz, M. An Exact Method to Obtain Effective Electrostatic Interactions from Computer Simulations: The Case of Effective Charge Amplification. *J. Chem. Phys.* **2013**, *139*, 064709.